Journal of Biomolecular NMR (2006) 36: 55–71
DOI 10.1007/s10858-006-9070-5
© Springer 2006

Article

Magic-angle spinning solid-state NMR of a 144 kDa membrane protein complex: *E. coli* cytochrome bo_3 oxidase

Heather L. Frericks[a,†], Donghua H. Zhou[a], Lai Lai Yap[b,†], Robert B. Gennis[a,b,c] & Chad M. Rienstra[a,b,c,*]

[a]*Department of Chemistry, University of Illinois at Urbana-Champaign, 600 South Mathews Avenue, Urbana, IL 61801, USA;* [b]*Department of Biochemistry, University of Illinois at Urbana-Champaign, 600 South Mathews Avenue, Urbana, IL 61801, USA;* [c]*Center for Biophysics and Computational Biology, University of Illinois at Urbana-Champaign, 600 South Mathews Avenue, Urbana, IL 61801, USA*

Received 4 April 2006; Accepted 24 July 2006

Key words: chemical shift, correlation spectroscopy, membrane protein, recoupling, sample preparation, secondary structure

Abstract

Recent progress in magic-angle spinning (MAS) solid-state NMR (SSNMR) has enabled multidimensional studies of large, macroscopically unoriented membrane proteins with associated lipids, without the requirement of solubility that limits other structural techniques. Here we present initial sample preparation and SSNMR studies of a 144 kDa integral membrane protein, *E. coli* cytochrome bo_3 oxidase. The optimized protocol for expression and purification yields ~5 mg of the enzymatically active, uniformly ^{13}C,^{15}N-enriched membrane protein complex from each liter of growth medium. The preparation retains endogenous lipids and yields spectra of high sensitivity and resolution, consistent with a folded, homogenous protein. Line widths of isolated signals are less than 0.5 ppm, with a large number of individual resonances resolved in the 2D and 3D spectra. The ^{13}C chemical shifts, assigned by amino acid type, are consistent with the secondary structure previously observed by diffraction methods. Although the structure is predominantly helical, the percentage of non-helical signals varies among residue types; these percentages agree well between the NMR and diffraction data. Samples show minimal evidence of degradation after several weeks of NMR data acquisition. Use of a triple resonance scroll resonator probe further improves sample stability and enables higher power decoupling, higher duty cycles and more advanced 3D experiments to be performed. These initial results in cytochrome bo_3 oxidase demonstrate that multidimensional MAS SSNMR techniques have sufficient sensitivity and resolution to interrogate selected parts of a very large uniformly ^{13}C,^{15}N-labeled membrane protein.

Introduction

It is well-known that structural studies of membrane proteins have lagged behind the progress of their water-soluble counterparts, with only a fraction of structures available to date belonging to membrane proteins. Their hydrophobicity hinders the most widespread, atomic-resolution, structural techniques of X-ray crystallography and solution NMR. For example, the insolubility of membrane proteins makes optimization of crystallization conditions notoriously difficult (Pautsch

†Heather L. Frericks and Lai Lai Yap contributed equally to this work.

*To whom correspondence should be addressed. E-mail: rienstra@scs.uiuc.edu

et al., 1999; Fahem and Bowie, 2002; Caffrey, 2003), limiting the number that can be studied by X-ray crystallography. Some membrane proteins can also be examined by solution NMR; unfortunately, these experiments may require extensive optimization of membrane mimetic conditions, which are typically different than the conditions used for crystallography. The task of identifying suitable detergents for micelle or bicelle preparation can approach the difficulty of growing single crystals (Vinogradova et al., 1998; Sorgen et al., 2002). Both crystallography and solution NMR also are challenged by the fact that such sample preparation techniques may differ from the conditions observed in a cell membrane and therefore have less than ideal physiological relevance. In contrast, solid-state NMR (SSNMR) does not require single crystals or small soluble particles to obtain high-resolution data (Hiller et al., 2005; Lorch et al., 2005). This fact allows large enzymes to be readily studied under active conditions, as demonstrated by mechanistic studies of bacteriorhodopsin in native lipids (Harbison et al., 1983; Hu et al., 1995). These studies illustrate that site-resolved spectra of membrane-bound enzymes can be obtained in fully active preparations, by combining relatively low magnetic field instruments (200–400 MHz ^{1}H frequencies) with specifically labeled samples.

In recent years many laboratories have extended SSNMR studies to higher field instruments (500–800 MHz or greater ^{1}H frequencies), in order to employ site-resolved multidimensional spectra of uniformly ^{13}C,^{15}N-enriched protein samples for assignment and structure determination. With this motivation, numerous studies over the last decade have investigated the spectral resolution of microcrystalline proteins. Early work by Torchia and co-workers in staphylococcal nuclease demonstrated the agreement of solution and solid-state chemical shifts (Cole et al., 1988). More recent systematic studies by Zilm and co-workers proved that nano- or microcrystalline globular proteins, which show characteristic powder diffraction patterns but lack sufficient long-range order for single crystal diffraction, yield high resolution magic-angle spinning (MAS) SSNMR spectra (Martin and Zilm, 2003). Such resolution, combined with uniform ^{13}C^{15}N labeling and multidimensional experiments, led to complete chemical shift assignments of several water-soluble peptides and proteins in precipitated forms, including SH3 (Pauli et al., 2001), ubiquitin (Igumenova et al., 2004a, b) and thioredoxin (Marulanda et al., 2005). Likewise our laboratory has studied a small globular domain of protein G (β1 immunoglobulin binding domain, GB1) and observed especially high resolution (~0.1 ppm line widths in ^{15}N and ^{13}C dimensions of spectra at 500 MHz) in microcrystalline preparations (Franks et al., 2005). Together these studies arrive at the general conclusion that if a protein is properly folded, hydrated and microscopically ordered on the length scale of a few nanometers (10–30 Å), spectroscopic resolution will be limited primarily by instrumental factors; moreover, commercially available instrumentation is well-suited to such studies.

More recently, similar multidimensional MAS methods have been employed to examine extensively or uniformly enriched membrane proteins. Several recent examples demonstrate the progress in such applications. 2D proton driven spin diffusion ^{13}C–^{13}C correlation experiments elucidated the membrane bound conformation of colicin Ia (Luo et al., 2005). 2D ^{13}C–^{13}C and ^{15}N–^{13}C experiments were combined with uniform and selective biosynthetic isotope labeling of the light-harvesting complex 2 to assign the majority of the ^{13}C and ^{15}N chemical shifts in this large membrane protein (Egorova-Zachernyuk et al., 2001; van Gammeren et al., 2005). In bacteriorhodopsin, site resolution even at relatively low magnetic field strengths enabled the determination of the distances between the retinal Schiff base and neighboring aspartic acid residues (Jaroniec et al., 2001). These studies show that experiments can be performed on large membrane protein complexes to determine binding interactions (Krabben et al., 2004), mechanistic details (Hatcher et al., 2002) and structural information (Luo et al., 2005). The success of these experiments can be attributed to the hydrated environment and local order that is maintained in SSNMR samples, leading to high-resolution data.

Here we present initial studies of a very large membrane protein complex (144 kDa), the cytochrome bo_3 ubiquinol oxidase (cytochrome bo_3). This enzyme is a member of the heme-copper oxidase superfamily (Garciahorsman et al., 1994; Zaslavsky and Gennis, 2000) which includes the

mitochondrial cytochrome *c* oxidase. Cytochrome bo_3 catalyzes the four-electron reduction of oxygen to water while conserving most of the free energy in the form of a transmembrane electrochemical potential. At 144 kDa, cytochrome bo_3 is too large to be studied by conventional solution NMR methods, producing very broad resonances in proton spectra (Zhang et al., 2004). Studies by X-ray crystallography have yielded a 3.5 Å resolution structure (Figure 1). At this resolution, structural features and the majority of the residues can be identified, but many mechanistic details still remain unanswered. SSNMR is an ideal tool to further examine the missing information because it is capable of providing atomic-resolution of side chains, allowing mechanistic issues to be addressed. For instance, SSNMR can be utilized to determine protonation states and pK_a values of the amino acids involved in proton translocation (Thomas et al., 1993; Das et al., 2001). Studies can also be performed to confirm post-translation modifications, including the cross-link between His 284 and Tyr 288 (Uchida et al., 2004), and investigate chemical interactions occurring in the ubiquinol-binding site (Hellwig et al., 2002).

As a first step in this direction, here we demonstrate improved methods for expression of cytochrome bo_3 from isotopically labeled media, yielding several milligrams per liter of the active enzyme complex. We then compare methods of preparation for SSNMR analysis. Our preparation results in a fully active, functionally relevant state, in which the signal intensity and relaxation properties as a function of temperature are favorable for 2D and 3D studies, which are subsequently demonstrated and analyzed by secondary chemical shift and relative signal intensity. We address a number of technical issues that are essential for future SSNMR structural studies of such large complexes. Despite the high molecular weight of this complex, the results bode well for more detailed studies of structure and function by multidimensional SSNMR and the improved technical capabilities to pursue total structure determination of increasingly large membrane protein complexes by MAS methods.

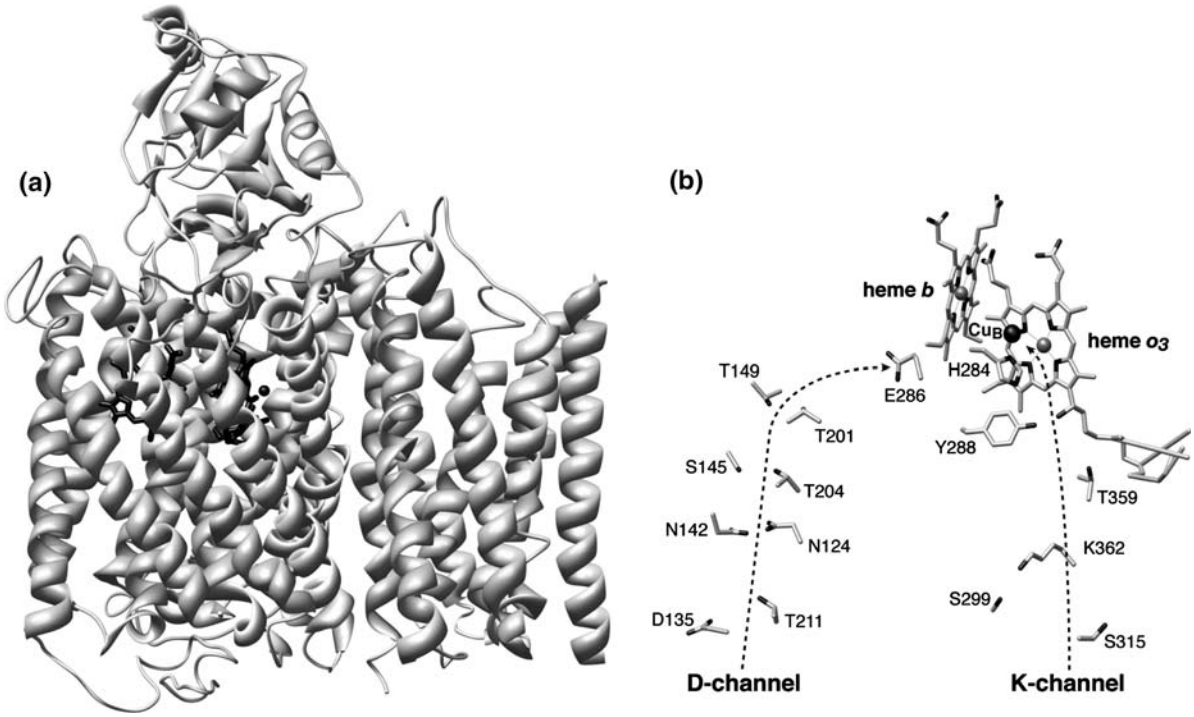

Figure 1. X-ray crystal structure of *E. coli* cytochrome bo_3 oxidase acquired by Abramson et al. (2000). (a) The complete structure is displayed with the heme o_3, heme b and Cu_B prosthetic groups highlighted. (b) The residues and prosthetic groups involved in the proton transfer pathways are displayed. The dashed lines indicate the path of water through the channels. Molecular graphics images were produced by the UCSF Chimera package (Pettersen et al., 2004).

Materials and methods

Sample 1: [^{13}C,^{15}N-Gly, uniform-^{15}N]

E. coli C43 (Avidis, France) cells contained the pJRHisA plasmid, which encodes the cyoABCDE operon expressing the wild type cytochrome bo_3 with a hexa-His affinity tag on the C-terminal domain of subunit II. Further details about this plasmid can be found in Rumbley et al. (1997). The cells were grown in a minimal medium containing 2-^{13}C,^{15}N-glycine (100 mg/l), ^{12}C-glycerol (2 g/l) and $^{15}NH_4Cl$ (2 g/l) as the sole carbon and nitrogen sources. The 1 l of minimal medium consisted of M63 salt solution (3 g KH_2PO_4, 7 g K_2HPO_4) supplemented with 1 mM $MgSO_4$, 10 μM $CuSO_4$, 30 μM $FeSO_4$ and 10 mg thiamine. Supplementation of these trace metals and vitamins was determined to be critical for heme production and increased the production of active enzyme, and the quantities were optimized accordingly on natural abundance growths. The subsequent purification steps, cell disruption by French press, solubilization in 1% *n*-Dodecyl β-D-maltoside (DM) detergent, followed by Ni^{2+} affinity chromatography, (Rumbley et al., 1997) yielded 10 mg cytochrome bo_3 from 5 l of growth media. Half of this sample (5 mg) was dialyzed against a total of 12 l of 25 mM Tris buffer, pH = 8.0, for 3 days to remove detergent. The sample was then pelleted using ultracentrifugation for 12 h at 180,000×*g*. This pellet, containing 5 mg of cytochrome bo_3, endogenous lipids and excess dialysis buffer to maintain a hydrated environment, was transferred into a 3.2 mm diameter, standard wall SSNMR rotor (22 μl sample volume; Varian NMR, Palo Alto, California). We refer to this as Sample 1a; its final composition by mass in the NMR rotor was approximately 25% protein, 5% lipids and 60% buffer (in excess, to fill the active volume of the rotor; the excess buffer, lacking detergent, did not change the amount of precipitated protein). In this case and others noted below, the absolute mass of protein was estimated with an upper bound determined by the amount of protein in solution prior to the dialysis and ultracentrifugation procedure, and a lower bound as determined by the integrated NMR signal intensity observed with a ^{13}C one pulse spectrum at equilibrium conditions, compared relative to protein standards of more precisely known quantity. This procedure reports the protein quantity within ±10% error, based on experience of several dozen samples examined this way in our laboratory.

The second half of this sample (5 mg), referred to as Sample 1b, was fully oxidized with potassium ferricyanide and further purified on a Diethylaminoethyl (DEAE) anion exchange column against a NaCl gradient, giving a final protein yield of 2–2.5 mg. The sample was then dialyzed and pelleted using the same procedure as the previous sample; its composition by mass in the NMR rotor was approximately 10% protein, 1% lipids and 90% buffer (again in excess, as noted above). After NMR analysis, the samples were redissolved in buffer/detergent (50 mM K_2HPO_4 (pH = 7.0), 0.1% DM) for assays of activity and prosthetic groups, as described below.

Sample 2: [U-^{13}C,^{15}N] cytochrome bo_3

The *cyo* operon was subcloned into the inducible pET17b vector, and protein was expressed in *E. coli* C43 in the medium described above, but using instead U-^{13}C-glycerol (2 g/l) as the carbon source. Over-expression proceeded for 4 h after induction by IPTG, yielding approximately 5 mg/l of purified cytochrome bo_3 (a final yield of 9 ± 1 mg for 2 l). The final composition by mass of this sample was approximately 35% protein, 10% lipid, and 55% buffer (in excess). Purification and sample preparation for SSNMR were performed as indicated for Sample 1a. Several 2D and 3D spectra were acquired with this sample, prior to deterioration under high power proton decoupling.

Sample 3: [U-^{13}C,^{15}N] cytochrome bo_3

Sample 3 was prepared in a similar method as Sample 2, but at a scale of 3 l minimal media, yielding 20 mg of U-^{13}C,^{15}N cytochrome bo_3. The final purified protein was divided into two SSNMR rotors: 14 mg was packed into a thin wall 3.2 mm rotor (36 μl sample volume) and 6 mg into a 3.2 mm standard wall rotor, with excess dialysis buffer to maintain hydration. The final composition by mass of this sample was ~50% protein, 13% lipid and 37% buffer; this was the highest concentration of protein we were able to pack into a rotor. These samples remained viable for several

weeks of data acquisition, and are stable for several months when stored at −80 °C, without noticeable changes in the ^{13}C CP-MAS spectra. We attribute this sample longevity to experimental conditions and instrumentation as described further below.

Activity assay, heme, quinone and phosphate analysis

Cytochrome bo_3 activity was assessed on a Clark-type oxygen electrode in a solution of 50 mM K_2HPO_4 (pH = 7.0), 0.1% DM and fully reduced ubiquinol-1, as a substrate, using methods described by Ma (1998). The heme analysis was performed with 10 nmol of protein prepared by same method as Sample 2 using the previously described procedure (Rumbley et al., 1997). Quinones were extracted and analyzed by HPLC from 10 nmol of Sample 2 prior to SSNMR analysis using the procedure described by Rumbley et al. (1997). The lipid to protein ratio was determined by phosphate analysis of 2.0 and 2.7 nmol of digested protein, purified by the same procedure as Sample 1a and 1b, respectively (Chen et al., 1956).

NMR spectroscopy

SSNMR experiments were performed at B_0 fields of 11.7 and 17.6 T on a 500 MHz (^1H frequency) Varian Infinity Plus spectrometer and a 750 MHz (^1H frequency) Varian Unity Inova, respectively. MAS rates were typically 11,111 Hz at 500 MHz, 16,666 Hz for standard wall rotors at 750 MHz and 12,500 Hz for thin wall rotors at 750 MHz. All pulse sequences consisted of a tangent ramped cross polarization (Meier, 1992) with TPPM decoupling (Bennett et al., 1995) applied during the acquisition and evolution periods. All 500 MHz data and a majority of the 750 MHz data were acquired with Varian Balun^{TM} ^1H–^{13}C–^{15}N 3.2 mm probes, with a subset of the 750 MHz data acquired with a Varian BioMAS^{TM} ^1H–^{13}C–^{15}N 3.2 mm probe (Stringer et al., 2005). The variable temperature gas was maintained at −50 °C with 100 scfh flow, the lowest temperature currently available with this narrow bore 750 MHz probe design. Additional experimental details are listed in the figure captions below.

Results and discussion

Sample preparation, enzymatic activity and homogeneity

Studies of membrane proteins often suffer from the limited quantity of protein that can be obtained from the over-expression in bacterial membranes. The problem is exacerbated when bacteria are grown in minimal media. Some commercially available labeled rich media, such as BioExpress (Cambridge Isotope Laboratories, Andover, Massachusetts), are known to improve yield of water-soluble proteins. In initial tests of cell growth and protein expression with BioExpress, we found decreased doubling times and increased cell density but poorer overall expression yield. We attribute this to the slow rate of protein insertion into the membrane and the limiting production of co-factors required for activity. Therefore, in all subsequent optimization steps we employed minimal media, supplemented with those metals determined to give optimal activity for cytochrome bo_3.

Initial cultures of *E. coli* GO105 in Luria broth yielded 1.5 ± 0.5 mg/l of cytochrome bo_3. By changing the host strain and adding a T7 promoter we increased the yield 3-fold, using growth conditions necessary to incorporate stable isotopes. The transformation of the pJRHisA plasmid into *E. coli* C43, a strain engineered to minimize the toxicity associated with membrane protein expression (Miroux and Walker, 1996), further increased the yield to 2.5 ± 0.5 mg/l of minimal media. Subsequently, the *cyo* operon was subcloned into an inducible pET17b vector, and then the enzyme was expressed in *E. coli* C43, yielding 5 mg of purified protein per liter of minimal media. One concern of expressing cytochrome bo_3 in a new host strain and under a new promoter is the previously observed cytochrome oo_3 species of this enzyme (Puustinen et al., 1992). This inactive species has been observed in various over-expressing *E. coli* strains. Therefore a heme analysis was performed on cytochrome bo_3 expressed in *E. coli* C43 from the pET17b vector. This resulted in a 1:1 mixture of heme b:heme o, consistent with the active cytochrome bo_3 species.

Samples 1a and 1b (described above) were prepared in order to test protein purification and sample packing for SSNMR analysis. The 1D ^{15}N

spectra (Figure 2) of these samples were compared, showing a 62% reduction in signal intensity of Sample 1b relative to Sample 1a. A portion of this signal reduction, such as in the amide region, occurs primarily due to the quantity of protein, 2.5–3 mg, lost during the second chromatography step. However, the signals of side-chain ^{15}N sites on His, Arg and Lys decreased by an even larger margin. For example, the Arg Nε/Arg Nη and Lys Nζ signals observed a 77 and 83% decrease in signal intensity in the Sample 1b. The His Nδ1 and Nε2 signals were barely observed above the noise in this same 1D ^{15}N spectrum but are much stronger in the spectrum of Sample 1a. We also observed a significant difference in the lipid to protein ratios between these preparations. The protein purified solely by Ni affinity chromatography gives a lipid to protein ratio of 49 to 1, as determined by phosphate analysis (Chen et al., 1956). The protein that was subject to a second, ion exchange purification step yielded a lipid to protein ratio of 21 to 1; this lipid loss was also observed in *R. sphaeroides* cytochrome *c* oxidase (Distler et al., 2004). Our interpretation is that the loss of lipids during the second purification step decreased the stability of the protein, as observed by the decreased ^{15}N intensities of the cationic side-chains (and overall less favorable cross polarization dynamics at the same experimental temperature). The association of native lipids with a membrane protein is critical for maintaining the protein in a rigid, stable conformation. Although the enzymatic activity was not affected by the anion exchange chromatography step, the loss of yield and lipids far outweigh the small gain in purity. The use of only a Ni^{2+} affinity chromatography step yields greater than 90% sample purity as judged by gel electrophoresis, and the analysis of the 2D SSNMR data below is consistent with the fact that the cytochrome bo_3 is the major constituent in the sample rotor. For example, analysis of the spectra assuming only the presence of the enzyme yields consistently good agreement with residue-specific secondary chemical shifts, as discussed further below.

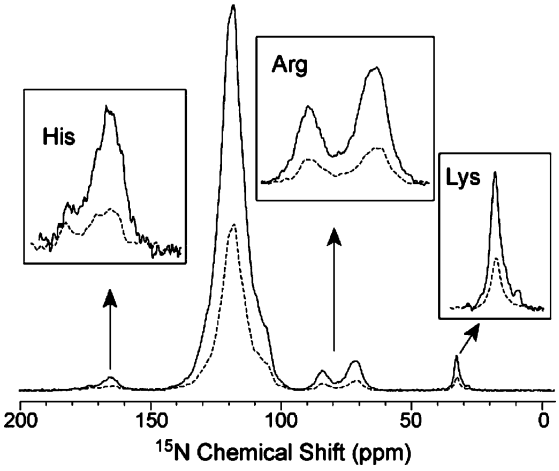

Figure 2. ^{15}N CP-MAS spectra of cytochrome bo_3, Sample 1a and 1b. Sample 1a (spectrum in solid lines) was purified by Ni^{2+} affinity chromatography. Sample 1b (dashed lines) was purified by Ni^{2+} affinity chromatography and anion exchange chromatography. Use of the anion exchange column resulted in a 62% loss in backbone amide signal and an even larger decrease in charged side-chain ^{15}N signals; enlargements of the His Nδ1 and Nε2, Arg Nε and Nη, and Lys Nζ regions show a respective 100, 77 and 83% decrease in signal intensity. 8,192 scans of each spectrum were acquired at 500 MHz ^1H frequency with a 11.111 kHz MAS rate and 70 kHz ^1H TPPM decoupling at −30 °C. The ^1H–^{15}N contact times (tangent ramp on ^{15}N) were 1.5 ms (Sample 1a) and 1.25 ms (Sample 1b). The spectra were processed with 30 Hz (0.6 ppm) Gaussian line broadening applied.

A major advantage of studying a membrane protein by SSNMR is that it can be prepared in near physiological conditions using mild sample preparation in native lipids, as demonstrated in previous mechanistic studies of bacteriorhodopsin (Hatcher et al., 2002) and R26 photosynthetic reaction center (Vanliemt et al., 1995). To ensure the sample preparation of cytochrome bo_3 yielded a stable, active enzyme, the absorption spectrum and the activity were monitored before and after SSNMR analysis. Before SSNMR analysis, Sample 1a gave a turnover rate of ~800 e-/s/enzyme, which is consistent with a fully active wild-type enzyme (Rumbley et al., 1997). The sample was then precipitated as described above and subjected to 8 days of data acquisition at 500 MHz (−30 °C). Following this treatment, the sample was solubilized and activity was reassessed. The activity was identical to the previous within the error of the method used. The retention of full activity following precipitation and SSNMR studies demonstrates that cytochrome bo_3 has most likely retained its native conformation throughout the procedure. We view the only alternative explanation (that the enzyme was denatured by the precipitation procedure and refolded upon solubilization) as exceedingly unlikely, given the known difficulty of refolding

membrane protein complexes. Moreover the SSNMR data directly report on the conformation of the protein in the precipitated state.

In addition to activity assays, the visible absorption spectrum of the enzyme was also monitored throughout the course of this work. Although the enzyme activity cannot be determined for the precipitated form of the protein, the red optical signature, characteristic of an active preparation of cytochrome bo_3, was observed both in the soluble and precipitated protein. The reduced minus oxidized difference spectra, acquired for each sample, displays a broad band centered at 562 nm, resulting from the absorption of the heme o and heme b irons. The presence of both of the hemes was further confirmed with the heme analysis, discussed above. A quinone analysis was also performed for this sample preparation protocol, on Sample 2 (8 mg U-$^{13}C^{15}N$ cytochrome bo_3) prior to SSNMR analysis. The quinone was extracted and analyzed by HPLC, demonstrating a ratio of cytochrome bo_3 to quinone of 1.0 to 0.9, as observed in other preparations of cytochrome bo_3 purified with DM (Rumbley et al., 1997). The mild solubilization and purification procedure used for preparing cytochrome bo_3 for SSNMR samples retained native lipids, hemes and quinone producing a near-physiological environment. The presence of the quinone in our preparation in particular, will allow for further investigation of this binding site, which is central to several unsolved mechanistic questions.

Temperature-dependent 1D spectra

Direct polarization (DP; i.e., Bloch decay spectra acquired at near-equilibrium conditions), cross polarization (CP) and ^1H T_1 inversion recovery MAS spectra were utilized to examine the spectral sensitivity and dynamics over a temperature range of -60 to -10 °C. We observed a 48% increase in total integrated intensity between -10 and -60 °C ^{13}C CP-MAS spectra. This increase in intensity has contributions both from the equilibrium ^{13}C and ^1H Boltzmann polarization and the CP efficiency (shown in Table 1). Specifically, as the temperature is lowered over this 50 °C range, the DP spectrum shows a 40% increase. Over this temperature range we observed a change in probe circuit tuning between -12 and -19 °C, due to the transition from liquid crystalline to gel phase lipids, which changes the sample conductivity and therefore the tuning of the probe circuit. Significantly below this phase transition, the DP sensitivity increases due to the larger Boltzmann polarization (i.e., 263/213 K = ~23%). In addition, the probe detection sensitivity improves marginally over this range. Another factor is the decrease in protein mobility, which results in improved CP dynamics; as confirmed in dipolar polarization transfer events, which took place with high efficiency at essentially the same mixing times that have been determined from microcrystalline model proteins (GB1 and ubiquitin) under the same experimental conditions (e.g., 1–1.5 ms for ^1H–^{15}N CP, ~1 ms for ^1H–^{13}C CP and 4–6 ms for ^{15}N to ^{13}C CP). ^1H inversion recovery experiments were also performed across this temperature range, showing a 30 ms increase in T_1 values from -10 to -60 °C, presumably due to decreased fast-limit motion of the side-chain and backbone atoms. The short ^1H T_1 values observed in this system for the bulk are due to the paramagnetic relaxation of protons near the heme sites, which subsequently spin-diffuse throughout the remainder of the complex; in contrast to the ~120–160 ms ^1H T_1

Table 1. Temperature dependence of signal intensities and relaxation rates

Nominal temperature† (°C)	^{13}C Bloch decay intensity*	CP intensity*	CP enhancement	^1H T_1 (ms)	Cα T_1 (s)	C′ T_1 (s)
−10	1.0	2.0	2.0	130	1.33	1.32
−30	1.2	2.4	2.0	140	1.22	1.36
−50	1.3	2.8	2.1	150	1.33	1.35
−60	1.4	3.0	2.2	160	1.27	1.32

*All spectra are normalized to the integrated intensity of the −10 °C Bloch decay spectrum. Spectra were acquired at 500 MHz ^1H frequency. †The nominal temperature is measured at the output of the variable temperature stack, with a flow rate of 100 scfh. Frictional heating from the spinning and dielectric heating from the RF pulses result in actual sample temperatures approximately 15–25 °C higher (Stringer et al., 2005; Li et al., 2006a).

values for cytochrome bo_3, we typically observe values on the order of 400–600 ms for other proteins in this temperature range. Rapid spin diffusion throughout the ^1H reservoir ensures that the entire protein has a uniform T_1 relaxation from this source. This relaxation mechanism is not as prominently observed in the ^{13}C T_1 values, which were ~1.3 s for the C′ and Cα spectral regions across the same temperature range. The ^{13}C relaxation of the methyl region is faster than the bulk, and therefore it appears spin diffusion from this source drives ^{13}C T_1 relaxation (Morcombe et al., 2005).

A temperature of −50 °C was chosen for further studies of cytochrome bo_3 at 750 MHz ^1H frequency. This is the lowest temperature that can currently be achieved on our 750 MHz instrument; lower temperatures potentially will offer additional improvements in sensitivity. At −50 °C the majority of large-scale backbone and side-chain motions appear to be frozen, as demonstrated by the improved sensitivity. This experimental temperature is comparable to conditions (−80 °C) under which the cytochrome bo_3 enzyme is stored for many months with minimal activity loss. As long as direct thermal damage from RF pulses can be avoided, we therefore expected this condition to extend the sample lifetime indefinitely. Consistent with this expectation, we were able to acquire a variety of multidimensional data sets at 750 MHz over the course of 6–8 weeks at −50 °C without sample deterioration, utilizing moderate ^1H decoupling fields (~70 kHz).

^{13}C CP-MAS experiments

The 1D ^{13}C CP-MAS spectrum at −50 °C (Figure 3) shows the expected peak intensities in each region of the spectrum, in qualitative agreement with the numbers of each residue type. Within each region of the 1D spectrum that was separately integrated (C′, Tyr Cζ, aromatic, Cα, Cβ and CH_3), the intensities are consistent with their expected relative values (Table 2), recognizing that the carbonyl and aromatic signals have lower intensities, due to the lower ^1H–^{13}C cross polarization (CP) efficiency and larger chemical shift anisotropy (CSA) that is commonly associated with these resonances. Overall the signal intensities in the protein are consistent with a rigid solid, where (^1H–^{13}C) CP efficiency along the backbone and side-chains is uniform, within our measurement error. The relative intensity of the first order carbonyl spinning side band at ~90 ppm is ~10% of the center band, which is also consistent with a rigid lattice backbone chemical shift anisotropy (CSA) magnitude at this MAS rate.

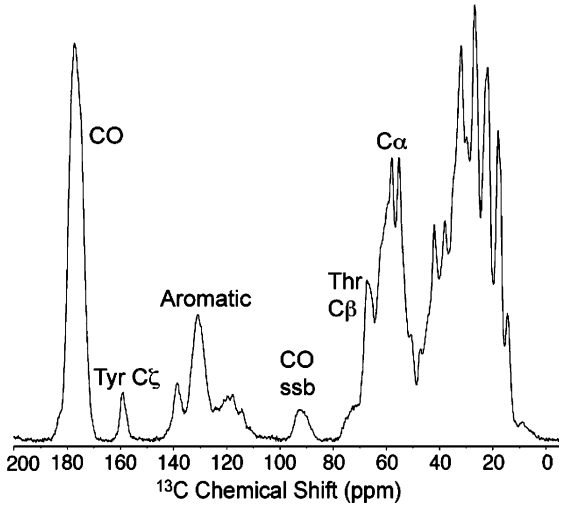

Figure 3. ^{13}C CP-MAS spectrum of cytochrome bo_3 (Sample 2, 55 nmol of uniformly $^{13}C^{15}N$-labeled). 768 scans were acquired at 750 MHz with a 16.666 kHz MAS rate and 73 kHz ^1H TPPM decoupling, −50 °C. The ^1H to ^{13}C contact time (^{13}C tangent ramp) was 0.8 ms. Data was processed with 30 Hz (~0.16 ppm) net line broadening (Lorentzian-to-Gaussian apodization) applied.

Table 2. Signal intensities by signal type in 1D ^{13}C CP-MAS spectra (−50 °C), at 750 MHz ^1H frequency

Signal type	# Signals (N)	Intensity (I)	Ratio (I/N)
Carbonyl	1,442	1,800	1.25
Tyr Cζ	38	88	2.30
Aromatic	1,297	780	0.80
Cα	1,290	2,610	2.02
Cβ	2,688	5,820	2.17
CH_3	3,978	8,430	2.12

The CP enhancement in this sample was observed to be ~1.7 (carbonyl and aromatic) to 2.3 (aliphatics) and the SPECIFIC (Baldus et al., 1998) double cross polarization (DCP) (Schaefer and Stejskal, 1979) efficiency is ~53% N-CO and ~43% N-Cα transfer efficiency on our 750 MHz instrument. This is similar to values we observe in small microcrystalline proteins such as ubiquitin

and GB1 (Franks et al., 2005). These observations, along with the chemical shift anisotropy (CSA) magnitudes of the C′ signals and the typical dependence of ^{13}C signal intensities and line widths on ^{1}H decoupling parameters, are all consistent with a protein preparation with little if any large-scale, global backbone motion.

2D ^{13}C–^{13}C correlation spectrum

Several 2D correlation spectra were acquired to test instrumental performance, the stability of the cytochrome bo_3 sample under high power pulsing, the chemical shift dispersion among amino acid types and to analyze the secondary structure based upon secondary chemical shifts. The ^{13}C–^{13}C 2D spectrum (Figure 4a), acquired with 25 ms DARR mixing (Takegoshi et al., 2001), shows peaks in all the expected locations, corresponding to correlations between backbone C′ and Cα, backbone (C′ and Cα) to side-chain (Cβ), and side-chain to side-chain. Several correlations are observed in isolated regions of the spectrum (e.g., Ala Cα-Cβ, Gly Cα-C′, Thr Cβ-Cγ, Ile Cα-Cγ2, etc.), providing a means to perform analysis of secondary structure and to gauge the underlying resolution of individual resonances. The relative integrated intensities observed in these isolated regions were consistent with expectations for each residue type, as described for the ^{13}C CP-MAS spectrum above; although transfer efficiencies are not perfectly uniform in DARR mixing spectra, comparisons of Gly, Ala, Ser, Thr and Val regions for example are quite reliable, since the 25 ms mixing time yields nearly complete transfer within these smaller spin systems. Spectra of model proteins were utilized to confirm this behavior. Further analysis within the unique chemical shift ranges of various residue types showed that the Cα, Cβ and C′ signals are observed with chemical shifts indicative of their secondary structure. For example, 73% of the Ala Cβ-Cα correlations (Figure 4b) are highly overlapped at ~55.5, 18 ppm, with ~2–3 ppm dispersion in each dimension. This is distinct from the Cα (52.5 ± 0.7 ppm) and Cβ ranges (19.0 ± 0.7 ppm) expected for a random coil Ala (Wishart and Sykes, 1994), and consistent with residues in an α-helical secondary structure environment. In addition,

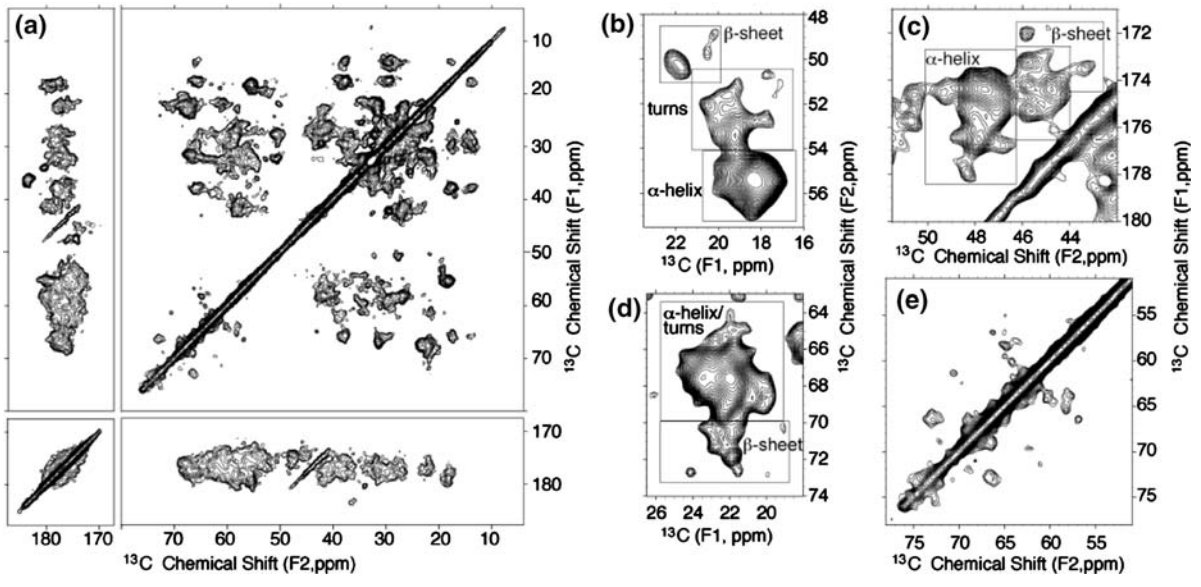

Figure 4. 2D ^{13}C–^{13}C correlation spectrum of cytochrome bo_3 (Sample 3, 100 nmol of uniform-$^{13}C^{15}N$) using 25 ms of DARR mixing acquired at 750 MHz using a Varian Bio-MAS^{TM} triple resonance (^{1}H–^{13}C–^{15}N) probe at a 12.5 kHz MAS rate. (a) Aliphatic and carbonyl regions. Secondary structure analysis was completed on the Ala Cβ-Cα (b), Gly Cα-C′ (c), Thr Cγ-Cβ (d) and Ile Cγ-Cα regions of the spectrum. Enlargements of each of these regions are shown (b)–(d) (except the Ile Cγ-Cα region) with the helical, turn and β-sheet residues indicated. The resolution of the spectrum is displayed in the Gly Cα-C′ (c) and Ser/Thr Cα-Cβ (e) regions, with numerous resolved single peaks with minimum line widths of 0.2 ppm. Data was acquired using 96 kHz ^{1}H TPPM (6.2 μs, 20°) for 14 ms during acquisition time and 14 ms during t_1 evolution time (−50 °C, 144 scans for 16 h of data acquisition with 0.5 s pulse delay). Data was processed with 47 Hz net line broadening and zero filling to 4096 (F1) × 8192 (F2) complex points.

several Ala signals are shifted to the upper left (upfield in the Cα dimension and downfield in the Cβ dimension) of this random coil range, consistent with β-sheet secondary structure. The peak at ~22, 50.2 ppm is consistent with Ala Cβ-Cα in a β-sheet; 5% of the total Ala intensity is expected to arise from four residues in the β-sheets in subunit I of cytochrome bo_3. The remaining 22% of the Ala intensity is observed at frequencies of F1 = 17–21 ppm and F2 = 54.1–51 ppm, encompassing the random coil values. Other isolated correlations of the spectrum (Gly C′-Cα (Figure 4c), Thr Cγ-Cβ (Figure 4d), Ile Cγ2-Cα) were integrated based on Chemical Shift Index (CSI) values for random coil, helix and β-sheet secondary structure elements and the grouping of peaks (Wishart and Sykes, 1994). The integrated areas and percentage of integrated intensity are shown in Table 3.

These secondary structure trends were compared to those given by the X-ray crystal structure of cytochrome bo_3 (Abramson et al., 2000). The structure was analyzed by the program DSSPcont, which classifies each residue to one of 10 secondary structure states based on hydrogen bonding and thermal fluctuations (Anderson et al., 2002). For the purpose of this work, the DSSPcont output was employed to classify each residue into one of three categories: helical, β-sheet or turn. The predicted secondary structure then was used to account for intensity observed in the SSNMR spectra. The 3_{10} (DSSPcont output of "G"), α ("H") and π ("I") helices give similar chemical shifts and are therefore classified together as helical residues. Likewise, the differences between antiparallel and parallel extended β-sheets cannot be discerned either from DSSPcont (grouped together with the result "E") or the isotropic chemical shift spectra. The remaining DSSPcont outputs were classified as turn residues: helical turns ("T"), β bridges ("B"), bends ("S"), and other ("L"). The number of helical, sheet and turn residues for each amino acid type was collected and compared to the integrated intensity of the ^{13}C–^{13}C spectrum regions in Table 3.

Table 3. Secondary structure analysis based on ^{13}C–^{13}C chemical shift spectra

Region	F1 (ppm)	F2 (ppm)	Percentage of integrated intensity[a]	Predicted percentage of structure[b]
Ala Cβ-Cα helical	54.1–57.4	16.7–20.3	73%	71%
Ala Cβ-Cα turns	50.4–54.1	17–21	22%	25%
Ala Cβ-Cα β-sheets	48.5–51.0	20–22.6	5%	4%
Gly Cα-C′ helical	173.4–183.5	46.2–50	65%	71%
Gly Cα-C′ turns	172.5–176.5	43.8–46.2	31%	27%
Gly Cα-C′ β-sheet	171.7–172.4, 173.1–173.9	42.8–43.8, 44.7–46.2	4%	2%
Thr Cγ-Cβ helical/turns	63.7–70.1	19.4–26.4	89%	94%
Thr Cγ-Cβ β-sheets	70.1–73.0	21.1–24.4	11%	6%
Ile Cγ2-Cα helical	16.0–19.5	63.7–67.8	85%	82%
Ile Cγ2-Cα turns	16.0–19.5	60.0–63.7	13%	11%
Ile Cγ2-Cα β-sheet	16.0–19.5	58.6–60.0	2%	7%
Ser Cα-Cβ helical[c]	122.5–127.7	60.2–64.5	68%	60%
Ser Cα-Cβ turns[c]	122–125.1	56.8–60.2	26%	34%
Ser Cα-Cβ β-sheet[c]	119.4–124.1	54.0–56.8	6%	6%
Thr Cα-Cβ helical[c]	133–141.4	63.8–70.3	78%	68%
Thr Cα-Cβ turns[c]	130.2–134.4	60.5–63.8	19%	26%
Thr Cα-Cβ β-sheet[c]	126.9–131.2	57.6–60.5	3%	6%

[a]Integration of isolated amino acid correlations in the ^{13}C–^{13}C spectrum, based on Chemical Shift Index (CSI) values for random coil, helix and β-sheet secondary structure elements (Wishart and Sykes, 1994). Integration was completed using the program Sparky (Goddard and Kneller, 2004) with a sum over box integration method using data at the 5σ contour level, where σ is the RMSD noise level. [b]Determined using DSSPcont for secondary structure analysis of the X-ray crystal structure, 1FFT.pdb. [c]Integration of a ^{13}C–^{13}C dipolar INADEQUATE spectrum using two supercycles of SPC-5 mixing (0.4 ms each) (Hohwy et al., 1999) at 500 MHz (data not shown). Integration was completed using the program Sparky (Goddard and Kneller, 2004) with a sum over box integration method using data at the 5σ contour level, where σ is the RMSD noise level.

This analysis shows that the relative integrated intensities of the helical, turn and β-sheet regions are in good agreement with the previously reported secondary structure in the crystal structure (Abramson et al., 2000). For example, the Ala Cβ-Cα correlation shows 73% of the intensity belonging to helical residues, versus the 71% of Ala determined to be helices in the crystal structure. Of the remaining Ala residues, 22% are predicted to be in a turn conformation and 4% in extended sheets. This is also in agreement with the ^{13}C–^{13}C spectrum with 25% of the intensity located in a random coil chemical shift range and 5% in a β-sheet. The Gly Cα-C′ and Ile Cγ2-Cα regions are also in good agreement with the predicted values from the crystal structure. In the standard DARR mixing spectrum, where the single quantum chemical shifts are correlated, the Cα–Cβ correlations of Ser and Thr residues in helical conformations typically appear very close to the diagonal. Therefore we acquired an additional INADEQUATE correlation spectrum (not shown) at 500 MHz to assess the secondary chemical shift trends of these residues. For Ser and Thr the percentage of helical structure observed was slightly higher than predicted. Overall, the observed secondary structure of the isolated correlations in the homonuclear ^{13}C–^{13}C spectra were consistent with that determined by the crystal structure.

In addition to the spectra displaying the anticipated secondary structure, many outlying resonances demonstrate the underlying resolution of the SSNMR spectra and of this sample preparation. For example, in many regions, individual peaks or small clusters of peaks can be observed, possessing narrow line widths (0.2–0.5 ppm) comparable to those observed to microcrystalline proteins (Martin and Zilm, 2003); if the sample lacked microscopic order, these line widths would be expected to be several ppm. In the Thr and Ser Cα-Cβ region (Figure 4e) of the DARR mixing spectrum, residues in β-sheets or turns are isolated from the near diagonal peaks of α-helical residues and are shown possessing substantial chemical shift dispersion. Good dispersion can also be observed in the Gly C′-Cα region (Figure 4c), including isolated peaks with chemical shifts consistent with β-sheet, turn and α-helical conformations. The isolated peaks typically arise from amino acids in unique structural contexts, such as β-sheet residues in a primarily α-helical membrane protein, or in unique chemical environment, which could include interactions with solvent or the active site. The presence of isolated peaks in a 2D spectrum, after only 16 h of data acquisition, demonstrate that additional multidimensional experiments have the potential to isolate the unresolved regions making identification of key cytochrome bo_3 residues possible.

^{15}N–^{13}C correlation spectra

The homonuclear ^{13}C–^{13}C spectrum above yields primarily intraresidue correlations, allowing for the identification of amino acid residue types. Heteronuclear ^{15}N–^{13}C correlation spectra provide inter-residue correlations, which are essential for making sequence-specific assignments (Hong, 1999). Therefore we next acquired 2D N-(C′)-CX and N-(Cα)-CX spectra on cytochrome bo_3. A backbone walk method is typically used to establish sequential assignments, by overlaying the spectra from both experiments to identify common ^{15}N resonances (Figure 5). Upon initial inspection of this data, it is obvious that further 3D experiments need to be completed in order to perform chemical shift assignments; nevertheless, even in these 2D data sets several isolated resonances are resolved. Similar to the ^{13}C–^{13}C experiment, those residues that give isolated resonances are likely to be in unique structural environments. An example of this can be observed for the Ser–Gly and the Gly–Gly pairs observed in the N-(C′)-CX experiment. In the cytochrome bo_3 sequence, there are 10 Ser-Gly pairs but only three of these pairs are located in a β-sheet or a turn. One of these, Ser 211-Gly 212 in Subunit II, is located in a random coil between two β-sheets on the exterior of the protein, exposed to solvent, in a different dielectric environment compared to the remainder of the protein; therefore a reasonable working hypothesis is that this residue pair gives rise to the isolated resonance. The chemical shifts of amide ^{15}N sites are known to depend strongly on amino acid type, backbone conformation, hydrogen bonding and electrostatics, giving additional information on the system studied (Oldfield, 2002; van Gammeren et al., 2005). Other isolated resonances can be observed in these spectra: Pro N-Cδ (129.5 ppm, 50.9 ppm), Arg Nη to Cζ (67.7 ppm, 158.8 ppm) and (74.5 ppm, 158.9 ppm) and Val or Thr N to Cγ (129.4 ppm, 22.9 ppm), (129.3 ppm, 21.3 ppm)

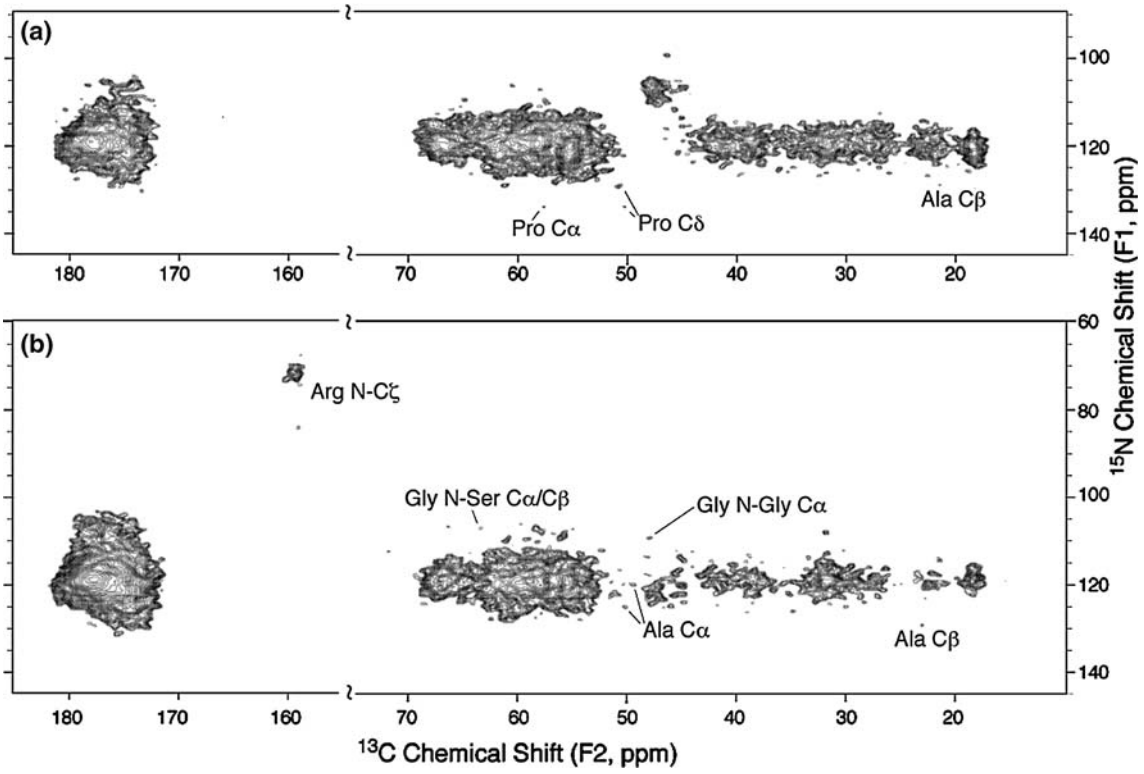

Figure 5. Heteronuclear ^{15}N–^{13}C 2D spectra of 55 nmol uniform-^{13}C^{15}N cytochrome bo_3 (Sample 2), showing several isolated resonances. (a) The ^{15}N-(^{13}Cα)-^{13}CX spectrum with 20 ms of DARR mixing was acquired for 160 scans with 13.3 ms of evolution time (113 kHz spectral width) in the indirect (^{15}N) dimension and 30 ms of acquisition in the direct dimension (^{13}CX). The carrier frequency was set to 55 ppm. (b) The ^{15}N-(^{13}C′)-^{13}CX was acquired with the same spectral resolution but the carrier frequency was set to 175 ppm and 25 ms of DARR mixing was used. Data was processed with 47 Hz (^{13}C) and 19 Hz (^{15}N) line broadening and shown at a level five times the RMS noise level.

and (127.1 ppm, 22.4 ppm). These isolated resonances are expected to be located in unique chemical environments.

3D N[i]-C′[i − 1]-CX[i − 1] correlation spectrum

^{15}N–^{13}C 2D correlation experiments are now well-established benchmarks in SSNMR for the assignment of backbone chemical shifts and ^{15}N–^{13}C–^{13}C 3D experiments are utilized to resolve overlapped resonances. In order to further resolve the degenerate chemical shifts that are common in α-helical proteins, a 3D N-C′-CX experiment was performed on cytochrome bo_3. Due to the large size of cytochrome bo_3, efforts were made to further improve the resolution and sensitivity of this experiment. It has been shown that line widths can be reduced and sensitivity improved if a rotor synchronized selective pulse is applied during the evolution period of a ^{13}C experiment (Li et al., 2006b; Zhou et al., 2006). This selective pulse removes the Cα-C′ scalar coupling, decreasing line widths and increasing Cα and C′ T_2 values. A selective 290 μs r-SNOB pulse (at the C′ frequency), followed by a hard π pulse was applied during the t_2 evolution period in the N-C′-CX 3D experiment (Figure 6). In addition to the application of selective decoupling to improve resolution, the N-C′-CX spectrum was acquired on a Varian Bio-MAS^{TM} probe. This scroll resonator probe significantly reduces the sample heating from radio frequency pulses by applying 16 times less dielectric heating per unit RF power than a solenoid coil probe (Stringer et al., 2005). The reduction in sample heating allowed for longer acquisition and evolution times (52.8 ms total), higher ^{1}H decoupling powers (88 kHz) and significantly shorter pulse delays (1 s) to be used in

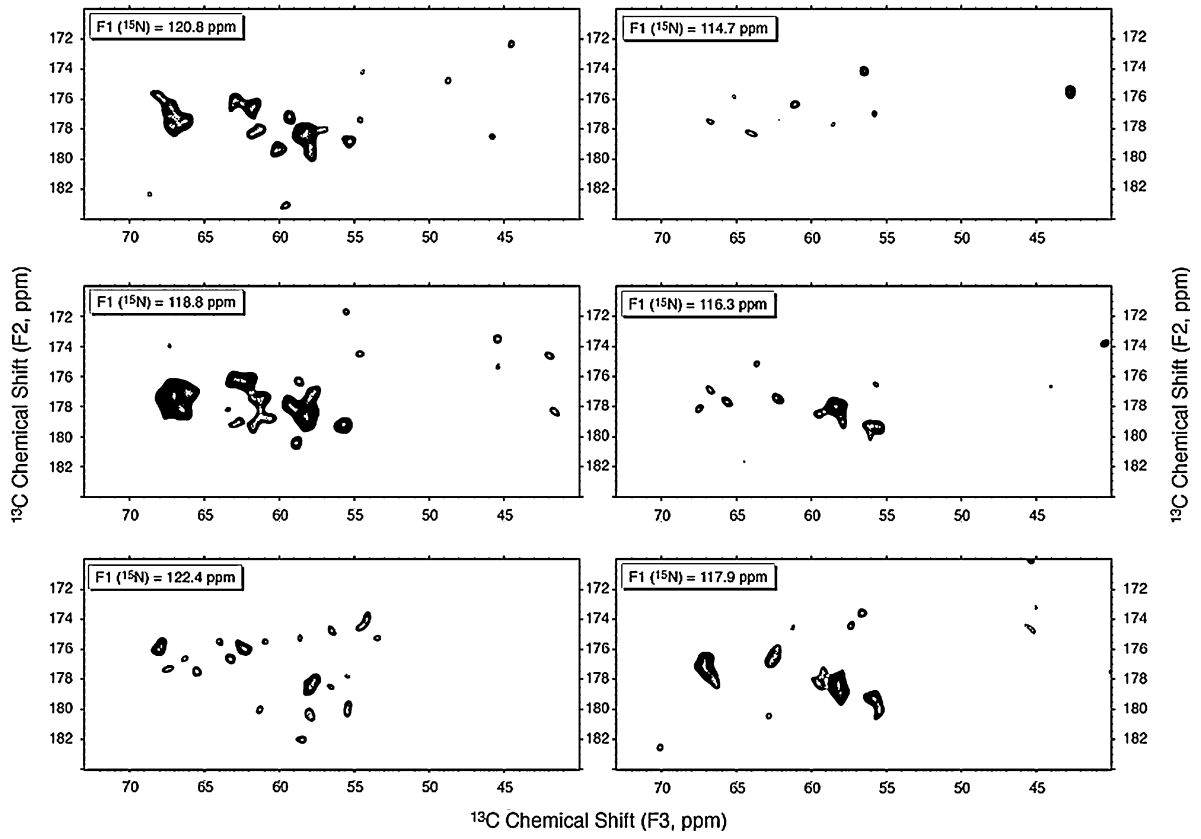

Figure 6. ^{15}N-^{13}C′-^{13}CX 3D spectrum of cytochrome bo_3 (100 nmol, Sample 3) at 750 MHz with 25 ms ^{13}C–^{13}C DARR mixing (−50 °C). The spectrum was acquired on the Varian Bio-MAS^{TM} scroll resonator probe to reduce sample heating, allowing a 1 s pulse delay to be utilized. A selective 290 μs r-SNOB pulse (at 175 ppm), followed by a hard π pulse was applied during the t_2 evolution period to decoupling the Cα and C′. Data was acquired with 96 rows in the in t_1 (^{15}N) dimension with a 160 μs dwell time (15.4 ms of evolution), 64 rows in t_2 (^{13}C′) dimension with a 160 μs dwell time (10.7 ms of evolution), and 26.7 ms of acquisition in the direct dimension (^{13}CX). The spectrum was processed with 115 Hz of line broadening in the ^{13}C dimensions and 50 Hz in the ^{15}N dimension, corresponding to a digital resolution of 0.6 ppm for ^{13}C signals and 0.7 ppm for ^{15}N resonances. (3 days of measurement time, 12 scans per row).

this experiment, further improving resolution and sensitivity. Initial attempts to perform experiments with a comparable duty cycle using solenoid coil designs resulted in thermal denaturation of the sample, even with a variable temperature gas set point of −50 °C with 100 scfh flow. With these techniques applied to the N-C′-CX experiment of cytochrome bo_3 numerous resolved resonances were detected.

Figure 6 show several F1 slices of the N-C′-CX spectrum of cytochrome bo_3, displaying the resolution observed for this 144 kDa membrane protein. In order to assess the overall number of peaks and the extent of resolution in this 3D spectrum, we used a conservative peak picking method as follows. The peaks were picked in C′-CX planes at a given ^{15}N frequency, displayed at a contour level of 5σ, where σ equals the RMS noise floor as calculated by Sparky 3.110 (Goddard and Kneller, 2004). For each C′-CX plane, incrementing the ^{15}N frequency every 0.5 ppm, the number of peaks was manually counted according to the following criteria: (a) For a given N-C′-Cα peak, there must be a N-C′-C′ peak observed with comparable intensity; in this transfer pathway, roughly half of the polarization from N to C′ should remain on the C′ site, with the remainder transferring to the side chain C sites. (b) The ^{13}Cα frequency must be between 43 and 72 ppm, corresponding to range of observed ^{13}C frequencies in the ^{13}C–^{13}C 2D experiments, and consistent with the typical range of Cα shifts in proteins (Seavey et al., 1991). (c)

For overlapped peaks, the relative peak intensity and the features in the shape of the peak was used to determine the number of overlapped peaks, assuming a unit peak intensity as determined by integration of resolved resonances. Using these criteria, 548 $^{13}C\alpha$ resonances were counted in the N-C′-CX 3D spectrum. This number is below the maximum number of 1,291 N-C′-Cα backbone resonances that would be observed for cytochrome bo_3 (i.e., neglecting other side-chain resonances that may show up from Asn, Gln, Arg, His and Trp residues in other regions of the spectrum), but the method used was very conservative to avoid selecting noise peaks and also underestimating the number of overlapped peaks.

To illustrate this point further, Figure 7 compares a ^{15}N plane of the N-C′-CX experiments displayed at 5.0σ, 4.5σ and 4.0σ. The signals

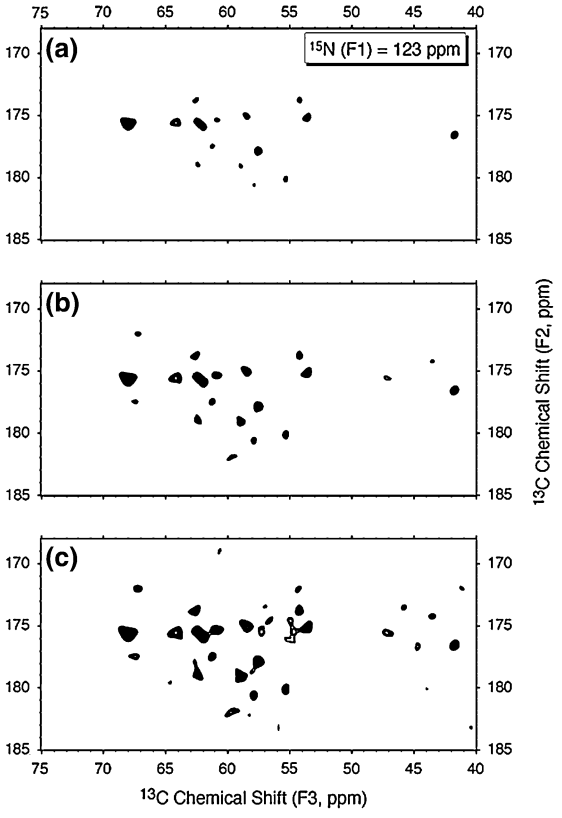

Figure 7. ^{15}N-($^{13}C'$)-^{13}CX 3D spectrum of cytochrome bo_3 (100 nmol, Sample 3) acquired at 750 MHz (−50 °C). The same spectrum as Figure 6 shown with (a) contours set to 5 σ (b) contours set to 4.5 σ and (c) 4 σ, with σ equaling the RMS noise level.

observed above the contour level of 5.0σ (Figure 7a) all appear in expected regions of the spectrum and match up with N-C′ peaks as described above. At lower contour levels, additional peaks throughout the Cα region are observed. Many of these appear again in regions of the spectrum where one would anticipate finding amino acid signals, with minimal intensity in other regions, such as >72 ppm or between 48 and 52 ppm, where there is a notch in the 1D ^{13}C spectrum. Examination of several other ^{15}N planes (not shown) gave similar results, resulting in an additional 30–40% peaks. Therefore the number of peaks estimated from the 5σ level analysis (548) is a lower bound on the actual total number of peaks above the noise threshold in this spectrum. Given the high resolution observed in the N-C′-CX experiment, we anticipate that a complete series of 3D ^{15}N–^{13}C–^{13}C and ^{13}C–^{13}C–^{13}C experiments will yield some site-specific assignments, and 4D experiments and/or modified isotopic labeling schemes (Lemaster and Cronan, 1982; Hong and Jakes, 1999) will be necessary to fully assign the chemical shifts in cytochrome bo_3.

3D ^{13}C–^{13}C–^{13}C correlation spectrum

The ^{15}N–^{13}C spectra are primarily utilized to assign backbone chemical shifts; however, due to the number of CP steps required to transfer from ^{1}H to ^{15}N to ^{13}C, the signal intensity is significantly decreased before polarization reaches side-chain ^{13}C resonances. In cytochrome bo_3, as with most enzymes, the majority of the mechanistic steps occur at charged or polar side chains; this includes proton translocation at Asp and Glu residues and metal ligation between His and Tyr residues. In order to isolate and assign the chemical shifts of these side chains carbons for further study of the cytochrome bo_3 catalytic mechanism, a ^{13}C–^{13}C–^{13}C 3D experiment was performed to resolve side-chain ^{13}C resonances. This experiment is an excellent tool to study these residues, due to the one step ^{1}H–^{13}C polarization transfer to all aliphatic carbons and the large chemical shift dispersion (~200 ppm) that is achieved by observing the ^{13}C resonances. The ^{13}C–^{13}C–^{13}C experiment, shown in Figure 8, has the sensitivity and dispersion that is typical of a ^{13}C–^{13}C 2D experiment, but with the ability to provide additional information in a third dimension. This particular

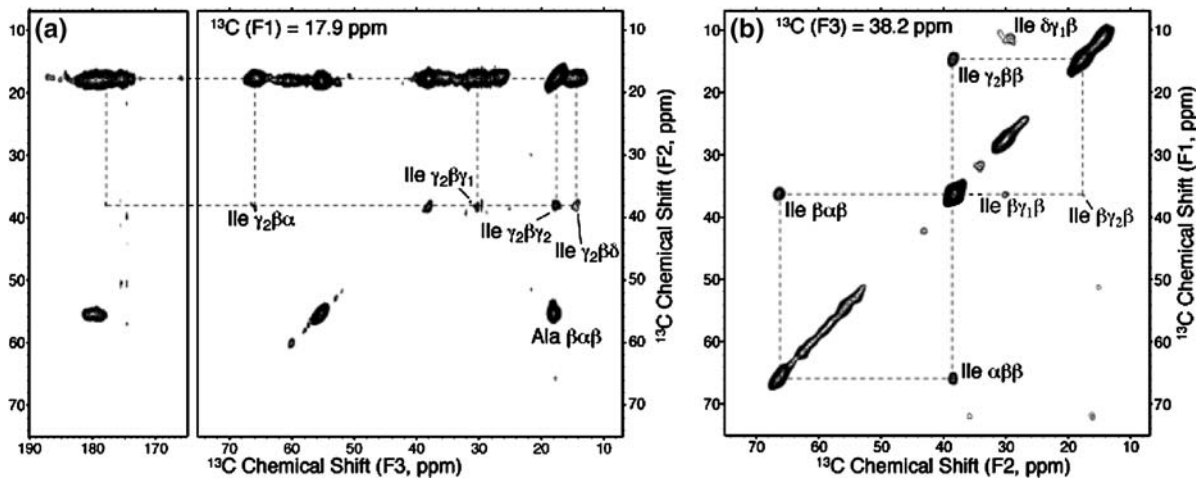

Figure 8. ^{13}C–^{13}C–^{13}C 3D spectrum of cytochrome bo_3 (55 nmol, Sample 2) showing long range connectivities in the F3 dimension and short range connectivities in the F2 dimension. (a) Long-range connectivities between Ile Cγ2 (F1 = 17.9 ppm) and Ile Cβ, Cα, Cγ1, Cδ and C′ are observed in the F3 dimension. (Ala Cβ-Cα correlations are also observed at this F1 frequency.) Additional information about this spin system is resolved in the F2 dimension, showing short-range correlations between Ile Cγ2 and Ile Cβ and Cα. (b) The spectrum shown at the Ile Cβ frequency (F3 = 38.2 ppm), further resolving the Ile spin system. The spectrum was acquired with 10 ms of DARR mixing after the t_1 evolution and 50 ms of DARR mixing after the t_2 evolution and 16.7 kHz spectral width in F2 and 33.3 kHz in F3 with a 7.5 ms evolution time in the indirect dimensions (− 50 °C, 16,666 Hz MAS). Twenty scans per row were acquired in 6 days (2.5 s pulse delay).

spectrum of cytochrome bo_3 was acquired with two DARR mixing periods, 10 ms between the F1 and F2 dimensions and 50 ms between the F2 and F3 dimensions, to distinguish between short-range and long-range interactions in a single experiment. Figure 8a displays long-range connectivities between Ile Cγ2 and Ala Cβ, including a correlation between Ile Cγ2, Cβ and Cα at (F1, F2, F3) = (17.9, 38.2, 66.5 ppm). The chemical shifts of the residues involved in this correlation can be further resolved in a third dimension, as shown in Figure 8b, displaying Ile Cβ short-range correlations. Although this experiment has the potential to ease the identification of peaks belonging to the same residues, this spectrum was not adequately digitized due to the very large bandwidth acquired in each indirect dimension. These limitations can be avoided by 3D techniques recently developed in our laboratory (Zhou et al., 2006), which utilize band-selective coherence transfer and scalar decoupling to reduce bandwidths and therefore experiment times.

Conclusions

We have demonstrated methods for the efficient production and SSNMR analysis of uniformly ^{13}C,^{15}N-labeled cytochrome bo_3. The optimized sample preparation involves a single column purification and dialysis for precipitation, yielding large quantities of enzyme in an active conformation with native lipids present. The rigid, homogenous and hydrated environment of the cytochrome bo_3 preparation produces multidimensional SSNMR spectra with narrow linewidths and high sensitivity. The spectra show chemical shifts consistent with the secondary structure previously reported by crystallography, but with some changes that may arise from the fact that portions of the protein were missing from the single crystal diffraction data. The use of multidimensional SSNMR experiments resolves a number of resonances, demonstrating that selected portions of this large membrane protein can be studied by SSNMR.

To complement the 3.5 Å X-ray structure of cytochrome bo_3 (Abramson et al., 2000), SSNMR is capable of answering detailed mechanistic questions by adding site-specific information at a level of chemical detail relevant to function, including the protonation states of residues, side-chain conformation and information about dynamics. The relaxed requirements for sample preparation in SSNMR permit large latitude in the choice of experimental conditions. For example,

the SSNMR can be performed at different pH values, allowing determination of the pK_a values of all assigned residues. Also, different reaction states of the enzyme can be studied by SSNMR. The *E. coli* quinol oxidase provides an excellent test case. The SSNMR data can be interpreted with knowledge of the approximate structure, and the information used to enhance the value of the structure to improve the understanding of function.

Although site-specific assignments were not yet possible in the current study, our results demonstrate that many individual resonances in a very large membrane protein complex can be resolved by 2D and 3D MAS methods, which is the first challenging step on the path to full assignments and structure determination. Further improvements in both data acquisition and interpretation methods are anticipated that will enable site-specific analysis in future studies.

Acknowledgments

The funding for this work was provided by the University of Illinois (startup funds to C.M.R.), the NIH & NIGMS Roadmap Initiative (GM075937-01), and an Ullyot Fellowship to H.F. The authors would like to thank Dr. Paul Molitor (VOICE NMR Facility of School of Chemical Science, University of Illinois) for technical support and Drs. John Stringer and Charles Mullen (Varian, Inc.) for assistance with installation of the 750 MHz scroll resonator probe.

References

Abramson, J., Riistama, S., Larsson, G., Jasaitis, A., Svensson-Ek, M., Laakkonen, L., Puustinen, A., Iwata, S. and Wikstrom, M. (2000) *Nat. Struct. Biol.* **7**, 910–917.

Anderson, C.A.F., Palmer, A.G., Brunak, S. and Rost, B. (2002) *Structure* **10**, 175–184.

Baldus, M., Petkova, A.T., Herzfeld, J.H. and Griffin, R.G. (1998) *Mol. Phys.* **95**, 1197–1207.

Bennett, A.E., Rienstra, C.M., Auger, M., Lakshmi, K.V. and Griffin, R.G. (1995) *J. Chem. Phys.* **103**, 6951–6958.

Caffrey, M. (2003) *J. Struct. Biol.* **142**, 108–132.

Chen, P.S., Toribara, T.Y. and Warner, H. (1956) *Anal. Chem.* **28**, 1756–1758.

Cole, H.B.R., Sparks, S.W. and Torchia, D.A. (1988) *Proc. Natl. Acad. Sci.* **85**, 6362–6365.

Das, T.K., Tomson, F.L., Gennis, R.B., Gordon, M. and Rousseau, D.L. (2001) *Biophys. J.* **80**, 2039–2045.

Distler, A.M., Allison, J., Hiser, C., Qin, L., Hilmi, Y. and Ferguson-Miller, S. (2004) *Eur. J. Mass Spectrom.* **10**, 295–308.

Egorova-Zachernyuk, T.A., Hollander, J., Fraser, N., Gast, P., Hoff, A.J., Cogdell, R., de Groot, H.J.M. and Baldus, M. (2001) *J. Biomol. NMR* **19**, 243–253.

Fahem, S. and Bowie, J.U. (2002) *J. Mol. Biol.* **316**, 1–6.

Franks, W.T., Zhou, D.H., Wylie, B.J., Money, B.G., Graesser, D.T., Frericks, H.L., Sahota, G. and Rienstra, C.M. (2005) *J. Am. Chem. Soc.* **127**, 12291–12305.

Garciahorsman, J.A., Barquera, B., Rumbley, J., Ma, J.X. and Gennis, R.B. (1994) *J. Bacteriol.* **176**, 5587–5600.

Goddard, T.D. and Kneller, D.G. (2004) Sparky 3.110 University of California, San Francisco.

Harbison, G.S., Herzfeld, J. and Griffin, R.G. (1983) *Biochemistry* **22**, 1–5.

Hatcher, M.E., Hu, J.G.G., Belenky, M., Verdegem, P., Lugtenburg, J., Griffin, R.G. and Herzfeld, J. (2002) *Biophys. J.* **82**, 1017–1029.

Hellwig, P., Yano, T., Ohnishi, T. and Gennis, R.B. (2002) *Biochemistry* **41**, 10675–10679.

Hiller, M., Krabben, L., Vinothkumar, K.R., Castellani, F., van Rossum, B.J., Kuhlbrandt, W. and Oschkinat, H. (2005) *Chem. Bio. Chem.* **6**, 1679–1684.

Hohwy, M., Rienstra, C.M., Jaroniec, C.P. and Griffin, R.G. (1999) *J. Chem. Phys.* **110**, 7983–7992.

Hong, M. (1999) *J. Biomol. NMR* **15**, 1–14.

Hong, M. and Jakes, K. (1999) *J. Biomol. NMR* **14**, 71–74.

Hu, J.G., Sun, B.Q., Griffin, R.G. and Herzfeld, J. (1995) *Biophys. J.* **68**, A332 .

Igumenova, T.I., McDermott, A.E., Zilm, K.W., Martin, R.W., Paulson, E.K. and Wand, A.J. (2004a) *J. Am. Chem. Soc.* **126**, 6720–6727.

Igumenova, T.I., Wand, A.J. and McDermott, A.E. (2004b) *J. Am. Chem. Soc.* **126**, 5323–5331.

Jaroniec, C.P., Lansing, J.C., Tounge, B.A., Belenky, M., Herzfeld, J. and Griffin, R.G. (2001) *J. Am. Chem. Soc.* **123**, 12929–12930.

Krabben, L., van Rossum, B.J., Castellani, F., Bocharov, E., Schulga, A.A., Arseniev, A.S., Weise, C., Hucho, F. and Oschkinat, H. (2004) *FEBS Lett.* **564**, 319–324.

Lemaster, D.M. and Cronan, J.E. (1982) *J. Biol. Chem.* **257**, 1224–1230.

Li, C., Mo, Y., Hu, J., Chekmenev, E.Y., Tian, C., Gao, F.P., Fu, R., Gor'kov, P.L., Brey, W.W. and Cross, T.A. (2006a) *J. Mag. Res.* **180**, 51–57.

Li, Y., Wylie, B.J. and Rienstra, C.M. (2006b) *J. Mag. Res.* **179**, 206–216.

Lorch, M., Fahem, S., Kaiser, C., Weber, I., Mason, A.J., Bowie, J.U. and Glaubitz, C. (2005) *Chem. Bio. Chem.* **6**, 1693–1700.

Luo, W.B., Yao, X.L. and Hong, M. (2005) *J. Am. Chem. Soc.* **127**, 6402–6408.

Ma, J.X., Puustinen, A., Wikstrom, M. and Gennis, R.B. (1998) *Biochemistry* **37**, 11806–11811.

Martin, R.W. and Zilm, K.W. (2003) *J. Magn. Reson.* **165**, 162–174.

Marulanda, D., Tasayco, M.L., Cataldi, M., Arriaran, V. and Polenova, T. (2005) *J. Phys. Chem. B* **109**, 18135–18145.

Meier, B.H. (1992) *Chem. Phys. Lett.* **188**, 201–207.

Miroux, B. and Walker, J.E. (1996) *J. Mol. Biol.* **260**, 289–298.

Morcombe, C.R., Gaponenko, V., Byrd, R.A. and Zilm, K.W. (2005) *J. Am. Chem. Soc.* **127**, 397–404.

Oldfield, E. (2002) *Ann. Rev. Phys. Chem.* **53**, 349–378.

Pauli, J., Baldus, M., van Rossum, B., de Groot, H. and Oschkinat, H. (2001) *Chem. Bio. Chem.* **2**, 272–281.

Pautsch, A., Vogt, J., Model, K., Siebold, C. and Schulz, G.E. (1999) *Proteins* **34**, 167–172.

Pettersen, E.F., Goddard, T.D., Huang, C.C., Couch, G.S., Greenblatt, D.M., Meng, E.C. and Ferrin, T.E. (2004) *J. Comput. Chem.* **25**, 1605–1612.

Puustinen, A., Morgan, J.E., Verkhovsky, M., Thomas, J.W., Gennis, R.B. and Wikstrom, M. (1992) *Biochemistry* **31**, 10363–10369.

Rumbley, J.N., Nickels, E.F. and Gennis, R.B. (1997) *Biochim. Biophys. Acta* **1340**, 131–142.

Schaefer, J. and Stejskal, E.O. (1979) *J. Magn. Reson.* **34**, 443–447.

Seavey, B.R., Farr, E.A., Westler, W.M. and Markley, J.L. (1991) *J. Biomol. NMR* **1**, 217–236.

Sorgen, P.L., Cahill, S.M., Krueger-Koplin, R.D., Krueger-Koplin, S.T., Schenck, C.C. and Girvin, M.E. (2002) *Biochemistry* **41**, 31–41.

Stringer, J.A., Bronnimann, C.E., Mullen, C.G., Zhou, D.H., Stellfox, S.A., Li, Y., Williams, E.H. and Rienstra, C.M. (2005) *J. Magn. Reson.* **173**, 40–48.

Takegoshi, K., Mizokami, J. and Terao, T. (2001) *Chem. Phys. Lett.* **341**, 540–544.

Thomas, J.W., Puustinen, A., Alben, J.O., Gennis, R.B. and Wikstrom, M. (1993) *Biochemistry* **32**, 10923–10928.

Uchida, T., Mogi, T., Nakamura, H. and Kitagawa, T. (2004) *J. Biol. Chem.* **279**, 53613–53620.

van Gammeren, A.J., Hulsbergen, F.B., Hollander, J.G. and de Groot, H.J.M. (2005) *J. Biomol. NMR* **31**, 279–293.

Vanliemt, W.B.S., Boender, G.J., Gast, P., Hoff, A.J., Lugtenburg, J. and Degroot, H.J.M. (1995) *Biochemistry* **34**, 10229–10236.

Vinogradova, O., Sonnichsen, F. and Sanders, C.R. (1998) *J. Biomol. NMR* **11**, 381–386.

Wishart, D.S. and Sykes, B.D. (1994) *J. Biomol. NMR* **4**, 171–180.

Zaslavsky, D. and Gennis, R.B. (2000) *Biochim. Biophys. Acta* **1458**, 164–179.

Zhang, J., Osborne, J.P., Gennis, R.B. and Wang, X.T. (2004) *Arch. Biochem. Biophys.* **421**, 186–191.

Zhou, D.H., Kloepper, K.D., Winter, K.A. and Rienstra, C.M. (2006) *J. Biomol. NMR* **34**, 245–257.